TECHNISCHE MECHANIK, 32, 6, (2012), 667 – 683
submitted: October 17, 2011

Some New Aspects of the Invariants of the Rate of Deformation Tensor and their Application on Viscoelastic Polymer Melts

A. Abid (Al-Baldawi), O. Wünsch

Non-Newtonian fluids, such as polymer melts, are modeled with viscoelastic models. In this work the use of the anisotropic mobility tensor of Giesekus and Phan Thien and Tanner in order to generalize the Maxwell model is discussed. Similarities in one-dimensional flows are needed to reproduce real fluid behavior under shear and elongation deformations. But the fact of different anisotropic mobility tensors in the models shows that there are also differences in two and three-dimensional viscoelastic flows. Therefore, we introduce a flow type parameter, using the invariants of the rate of deformation tensor. Here, the flow type is fully independent of the material model and therefore universally deployable. The numerical framework is done with OpenFOAM a Finite Volume based library. The stabilization of the simulations is carried out applying the Viscous Formulation and the Discrete Elastic Viscous Stress Splitting methods. A 4:1 contraction benchmark is done over a wide range of the Deborah number in order to show the stability of the methods used. Furthermore, the flow type parameter is applied on a Cross-Slot geometry. Here, the influence of the elasticity on the Euler velocity field and the rate of deformation tensor are shown to be dependent on the model used.

1 Introduction and Viscoelastic Modeling Approaches

In many fields of engineering processes, numerical simulations are used to predict the fluid flow in new designs of technical apparatus. Along with the complex geometries, the behavior of highly viscous fluids complicates the calculations. Fluids like polymer melts show not only viscous but also elastic properties which can influence the flow pattern in a dramatic manner. For instance, the fabrication of polymer sheets is usually started in a screw extruder, and the simulation is influenced if elasticity is taken into account, see Wünsch (2009).
In order to describe the real material behavior it is necessary to use models that relate the polymer part of the extra stress Tensor $\mathbf{T}_\mathrm{p}$ to the material time derivative of the Green's strain tensor $\dot{\mathbf{E}}$, respectively the rate of deformation tensor $\mathbf{D}$. Most models in literature specify this relation in a phenomenological way, see Thien (1978); Thien and Tanner (1977); Giesekus (1982); Bird et al. (1987); Böhme (2000).
In order to describe fluids with memory effects, an integral relationship over the time history is possible. Under some assumptions (isotropic material behavior, incompressibility, linear relation in the stress tensor and fading memory), a Walters Fluid A results. It can be written in the form

$$\mathbf{T}_\mathrm{p} = \int_0^\infty K(s) \frac{\mathrm{D}\mathbf{E}(t-s)}{\mathrm{D}s}\,\mathrm{d}s. \tag{1}$$

The relaxation function $K(s)$ depends on the retarded time s. When a specified function $K(s) = 2\eta_\mathrm{p}/\lambda e^{-s/\lambda}$ and a point in the past time $\tilde{t} = t - s$ depending of the current time t are introduced, eq. (1) leads to

$$\mathbf{T}_\mathrm{p} = \frac{2\eta_\mathrm{p}}{\lambda} e^{-t/\lambda} \int_{-\infty}^{t} e^{\tilde{t}/\lambda} \mathbf{F}_{\tilde{t}}^{-\mathrm{T}}(t)\mathbf{D}(\tilde{t})\mathbf{F}_{\tilde{t}}^{-1}(t)\,\mathrm{d}\tilde{t}. \tag{2}$$

Here η_p and λ are material parameters and $\mathbf{F}_{\tilde{t}}^{-1}$ and $\mathbf{F}_{\tilde{t}}^{-\mathrm{T}}$ denote the inverse of the relative deformation gradient and its transpose. Derivating eq. (2) with respect to the current time leads to the differential form of the contravariant Maxwell model, see Giesekus (1994). In order to expand the modeling possibilities of eq. (2), a generalized Maxwell model can be introduced as

$$\mathbf{T}_\mathrm{p} + \lambda \overset{\diamondsuit}{\mathbf{T}}_\mathrm{p} + \overset{(n)}{\mathbf{Q}}\big(\mathbf{T}_\mathrm{p}\big)\mathbf{T}_\mathrm{p} = 2\eta_\mathrm{p}\mathbf{D} + \tilde{\lambda}\overset{\triangledown}{\mathbf{D}}. \tag{3}$$

$\overset{(n)}{\mathbf{Q}}$ is a non-linear tensor function of different order and is called the anisotropic mobility tensor, $\tilde{\lambda}$ is an additional material constant. $\overset{\diamondsuit}{\mathbf{A}}$ and $\overset{\triangledown}{\mathbf{A}}$ denote objective time derivatives of an arbitrary tensor $\mathbf{A}$ and are defined as a Schowalter time derivative

$$\overset{\diamondsuit}{\mathbf{A}} = \overset{\triangledown}{\mathbf{A}} + \xi(\mathbf{AD} + \mathbf{DA}), \qquad \xi \in [0, 2]. \tag{4}$$

The upper convected Oldroyd time derivative, with $\xi = 0$, is given by

$$\overset{\triangledown}{\mathbf{A}} = \frac{\partial \mathbf{A}}{\partial t} + \nabla \cdot \left(\mathbf{v} \otimes \mathbf{A}\right) - (\nabla \mathbf{v})^{\mathrm{T}} \mathbf{A} - \mathbf{A} \nabla \mathbf{v}, \tag{5}$$

which is built with the gradient of the Euler velocity field $(\nabla \mathbf{v})^{\mathrm{T}}$ and its transpose. The parameter ξ controls the form of the time derivative. For $\xi = 1$, the Jaumann time derivative results and for $\xi = 2$, we get the lower convected Oldroyd time derivative. It is also possible to use a rational number inside the interval [0,2] for ξ. Note that the Newtonian fluid is also included in eq. (3) by setting $\lambda = \tilde{\lambda} = \overset{(n)}{\mathbf{Q}} = 0$.

Differential models are very comfortable to use with numerical implantation techniques. Differential models need only the current time to calculate the actual stress. By contrast, the integral models, e. g. eq. (1), require the whole time history to calculate the extra stress tensor. Nevertheless, using differential models leads to numerical difficulties because of the hyperbolic nature of the differential viscoelastic models, see Keyfitz and Shearer (1990) and Joseph and Yoo (1985). This leads to the formulations of splitting methods. In Rajagopalan et al. (1990); Joseph et al. (1985); Guéntte and Fortin (1995), stress splitting in a Newtonian solvent and polymer solvent is introduced (Viscous Formulation Method) in order to keep the ellipticity of the governing equations of continuity, momentum and hyperbolic constitutive model. Further developments are the Elastic Viscous Stress Splitting Method (EVSS) and Explicitly Elliptic Momentum Equation Method (EEME), that were introduced in Renardy (1985) and used in Jin et al. (1991) for a special type of differential models. All of the works mentioned above use Finite Elements Methods (FEM) to discretize the calculation domain. In recent literature the use of Finite Volume Methods (FVM) is increasing, see Xue et al. (1998) and Muniz et al. (2008). One benefit of the FVM techniques is that they handle the high element numbers in numerical meshes well. And a fine discretization is necessary to catch the elliptic properties, see Rajagopalan et al. (1990). In Alves et al. (2003), the FVM is used successfully in conjunction with the Viscous Formulation (VF). Two special material models (Oldroyd-B and Phan-Thien-Tanner (PTT)) are benchmarked with results of the literature over a wide range of viscoelastic properties, e. g. the Deborah number De.

The purpose of the present work is to provide numerical studies about the discretization methods that are used to solve viscoelastic fluid flows. A benchmark to Alves et al. (2003), Aboubacar et al. (2002) and Wünsch (2009) is done and will be elucidated later. To show differences between Giesekus and PTT fluids, we present two and three-dimensional simulations. In the case of 3D simulations, we used the invariants of the rate of deformation tensor $\mathbf{D}$ to introduce a new property to visualize the flow type. Here the difference to the Newtonian case is shown to be significant.

2 The Anisotropic Mobility Tensor Generalization

In the literature, many governing equations exist to describe the viscoelastic polymer part of the extra stress tensor $\mathbf{T}_{\mathrm{p}}$ as a function of the rate of deformation tensor $\mathbf{D}$ in a phenomenological way. Basically, the equations can be classified in models which are linear or nonlinear in the extra stress tensor. By way of example, the Oldroyd eight constant fluid Oldroyd (1950) and the Oldroyd with the Giesekus extension fluid (Giesekus (1994)) are mentioned. Furthermore, previous linear models, such as Maxwell-, Oldroyd- or Jeffrey fluids, are able to reproduce some rheological behavior. However, linear models show some weakness in decribing fluids like polymer melts. In order to model real fluid behavior for high deformation rates, additional nonlinear quantities in eq. (3) are necessary. Because of restrictions in the experimental identification, we prefer to describe material behavior with models that include as few parameters as possible. In the present work, the models of Giesekus (1982) and two types of Phan-Thien-Tanner-models (PTT) Thien (1978); Thien and Tanner (1977) are used with $\tilde{\lambda} = 0$ in eq. (3). These nonlinear additions $\overset{(n)}{\mathbf{Q}}\left(\mathbf{T}_{\mathrm{p}}\right)$ are described in Table 1. Note that for the Giesekus model, the additional function is tensorial and a scalar quantity in case of the PTT fluids. Furthermore, for an arbitrary tensor $\mathbf{A}$ the product is given by $(\mathbf{AA})_{\mathrm{ij}} = A_{\mathrm{im}} A_{\mathrm{mj}}$ and the trace of it is $\mathrm{tr}\left[\mathbf{A}\right] = A_{\mathrm{ii}}$. Here the new material parameter α is able to control the influence of the nonlinearity, such as shear thinning and elongational hardening in case of the Giesekus and the linear PTT fluids and even elongational softening for the exponential PTT fluids. The differences of the material models are visible in the flow behavior under rheometrical conditions. In the case of one-dimensional elongational

Table 1: Viscoelastic Fluid Modeling and the used anisotropic mobility tensors.

Non-linear tensor function $\overset{(n)}{\mathbf{Q}}$
Giesekus
$\mathbf{Q}(\mathbf{T}_\mathrm{p}) = \alpha\frac{\lambda}{\eta_\mathrm{p}}\mathbf{T}_\mathrm{p}$
PTT linear
$\mathrm{Q}(\mathbf{T}_\mathrm{p}) = \alpha\frac{\lambda}{\eta_\mathrm{p}}\mathrm{tr}[\mathbf{T}_\mathrm{p}]$
PTT exponential
$\mathrm{Q}(\mathbf{T}_\mathrm{p}) = \exp[\alpha\frac{\lambda}{\eta_\mathrm{p}}\mathrm{tr}[\mathbf{T}_\mathrm{p}]] - 1$
Parameter sets
Giesekus
$\mathbf{p}_\mathrm{G} = (\eta_\mathrm{p}, \lambda, \xi, \alpha)$
$\eta_\mathrm{p} > 0 \wedge \in \mathbb{R}; \quad \lambda > 0 \wedge \in \mathbb{R}; \quad \xi = 0; \quad \alpha \in (0, 1]$
PTT linear
$\mathbf{p}_\mathrm{L} = (\eta_\mathrm{p}, \lambda, \xi, \alpha)$
$\eta_\mathrm{p} > 0 \wedge \in \mathbb{R}; \quad \lambda > 0 \wedge \in \mathbb{R}; \quad \xi = \in [0, 1]; \quad \alpha \in [0, 2]$
PTT exponential
$\mathbf{p}_\mathrm{E} = (\eta_\mathrm{p}, \lambda, \xi, \alpha)$
$\eta_\mathrm{p} > 0 \wedge \in \mathbb{R}; \quad \lambda > 0 \wedge \in \mathbb{R}; \quad \xi = \in [0, 1]; \quad \alpha \in [0, 2]$

flow, the elongational viscosity is given with

$$\eta_\mathrm{D}(\dot{\varepsilon}) = \frac{\sigma_\mathrm{xx} - \sigma_\mathrm{yy}}{\dot{\varepsilon}} \quad \wedge \quad \lim_{\dot{\varepsilon}\to 0} \eta_\mathrm{D}(\dot{\varepsilon}) = 3\eta_\mathrm{p}. \tag{6}$$

with the first and second normal stress of the polymer part of the extra stress tensor σ_xx and σ_yy. In the limiting case of evanescent elongation rate $\dot{\varepsilon}$, the elongational viscosity turns into the threefold shear viscosity, which is known as Trouton phenomenon. The shear viscosity is given by

$$\eta_\mathrm{p}(\dot{\gamma}) = \frac{\sigma_\mathrm{xy}}{\dot{\gamma}} \quad \wedge \quad \lim_{\dot{\gamma}\to 0} \eta_\mathrm{p}(\dot{\gamma}) = \eta_\mathrm{p}, \tag{7}$$

with the shear stress σ_xy and the shear rate $\dot{\gamma}$. For vanishing shear rates the shear viscosity becomes a constant value. The majority of viscoelastic fluids show normal stress differences, see Hasseger et al. (2006). The normal stress coefficients are defined as

$$\nu_1 = \frac{\sigma_\mathrm{xx} - \sigma_\mathrm{yy}}{\dot{\gamma}^2} \quad \wedge \quad \nu_2 = \frac{\sigma_\mathrm{yy} - \sigma_\mathrm{zz}}{\dot{\gamma}^2}. \tag{8}$$

It can be shown that the first and second normal stress coefficients of the PTT-fluids are related to each other:

$$\nu_2 = -\frac{\xi}{2}\nu_1, \tag{9}$$

where ξ is the interpolation term of the G. Schowalter derivative, see (4).
The similarities and differences of elongational viscosities eq. (6) for the above-mentioned models are exemplarily shown for fixed nonlinear parameters (α and ξ) and normalized in Fig. 1. All curves start concertedly at small elongation rates related to eq. (6). For increasing elongational rates, Giesekus and PTT linear fluids show a hardening behavior and the elongational viscosity increases. For high elongation rates the elongational viscosity tends towards a constant value that depends on the parameter α. Here the exponential form of the PTT fluid is different, as the elongation viscosity shows softening behavior. For the case of adjusting the material parameters to describe the elongational behavior, as shown in Fig. 1, shear behavior diverges, see Dhanasekharan et al. (1999). This is due to the fact that the one-dimensional shear flow is set by four equations $(\sigma_\mathrm{xx}, \sigma_\mathrm{yy}, \sigma_\mathrm{zz}, \sigma_\mathrm{xy})$ and this increases the differences between the models. In Fig. 1 and Fig. 2 the shear thinning behavior of the shear viscosity is shown to be similar for small shear rates. Increasing the shear rate leads to a high shear thinning behavior in case of the Giesekus fluid. The exponential PTT fluid is bonded by the Giesekus and linear PTT fluids.

3 Visualization of the Flow Type in 3D Simulations

The calculation of fluid flows with viscoelastic material behavior in three-dimensional complex geometries is difficult due to the increasing expectations placed on the material model. Above all, it is necessary to choose a material

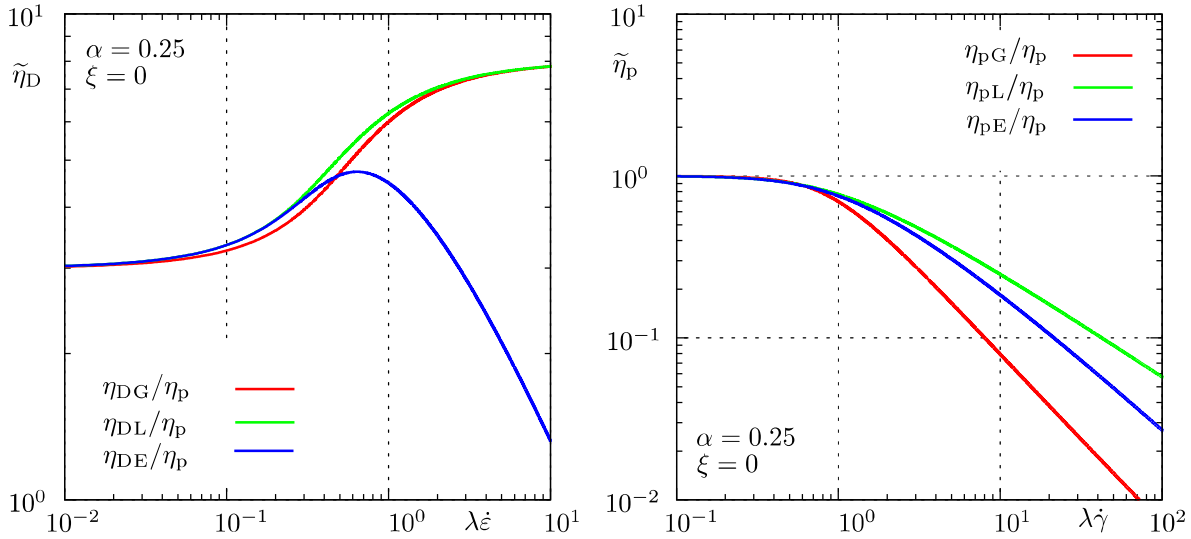

Figure 1: Normalized shear and elongational viscosity with the shear and elongation rate (Index: G - Giesekus, L - PTT linear, E - PTT exponential). Note the color version is available online.

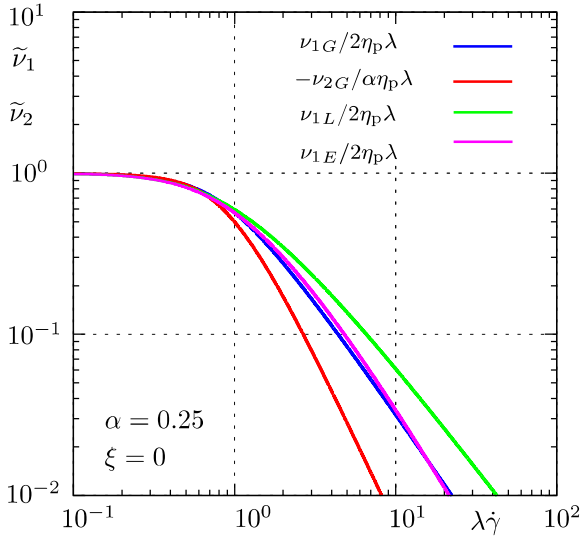

Figure 2: Normalized normal stress coefficients with the shear rate. Note the second stress coefficient of the PTT fluids is zero since ξ is set to zero (Index: G - Giesekus, L - PTT linear, E - PTT exponential).

model as elementary as possible which is able to desribe the whole material behavior properly. Therefore, it is helpful to know which kind of flow type dominates in the geometry.
In order to visualize the flow type, we use characteristic kinematic quantities: the invariants of the rate of deformation tensor $\mathbf{D}$. For a given fluid flow, the invariants are defined by the characteristic equation of the rate of deformation tensor, see Wünsch (2001) and Böhme (2000)

$$-\varphi^3 + \mathrm{I}_\mathbf{D}\varphi^2 - \mathrm{II}_\mathbf{D}\varphi + \mathrm{III}_\mathbf{D} = 0. \tag{10}$$

The first invariant is calculated by

$$\mathrm{I}_\mathbf{D} = \mathrm{tr}\big[\mathbf{D}\big] = 0, \tag{11}$$

which is zero for incompressible fluids. The second invariant is reduced to

$$\mathrm{II}_\mathbf{D} = -\frac{1}{2}\mathrm{tr}\big[\mathbf{D}\mathbf{D}\big]. \tag{12}$$

The third invariant is given by

$$\mathrm{III}_\mathbf{D} = \det\big[\mathbf{D}\big]. \tag{13}$$

It is well known that symmetric tensors involve real eigenvalues φ

$$\mathbf{D} = \mathbf{D}^\mathrm{T} \quad \rightarrow \quad \varphi \in \mathbb{R}. \tag{14}$$

Table 2: Values of κ for different flow types (e-f: elongational flow). Note that for uniaxial e-f the value of κ is positive and negative for biaxial e-f. Note that the with the sign we are able to differ between uniaxial and biaxial e-f.

Flow Type	Eigenvalues of $\mathbf{D}$	$-\mathrm{II}_{\mathbf{D}}$	$\mathrm{III}_{\mathbf{D}}$	κ
uniaxial e-f	$\dot{\varepsilon}_\mathrm{u}, -\dot{\varepsilon}_\mathrm{u}/2, -\dot{\varepsilon}_\mathrm{u}/2$	$\frac{3}{4}\dot{\varepsilon}_\mathrm{u}^2$	$\frac{1}{4}\dot{\varepsilon}_\mathrm{u}^3$	$\frac{2}{3\sqrt{3}}$
biaxial e-f	$\dot{\varepsilon}_\mathrm{b}, -2\dot{\varepsilon}_\mathrm{b}, \dot{\varepsilon}_\mathrm{b}$	$3\dot{\varepsilon}_\mathrm{b}^2$	$-2\dot{\varepsilon}_\mathrm{b}^3$	$-\frac{2}{3\sqrt{3}}$
planar e-f	$\dot{\varepsilon}_\mathrm{p}, -\dot{\varepsilon}_\mathrm{p}, 0$	$\dot{\varepsilon}_\mathrm{b}^2$	0	0
shear flow	$\dot{\gamma}/2, -\dot{\gamma}/2, 0$	$\frac{1}{4}\dot{\gamma}^2$	0	0

Now it is possible to introduce two new variables,

$$\Phi := -\left(\frac{\mathrm{III}_{\mathbf{D}}}{2}\right)^{-\frac{1}{3}} \varphi \tag{15}$$

and

$$\psi := \left(\frac{\mathrm{III}_{\mathbf{D}}}{2}\right)^{-\frac{2}{3}} \left(-\frac{\mathrm{II}_{\mathbf{D}}}{3}\right). \tag{16}$$

With (11), (15) and (16) we can rewrite (10) to

$$\Phi^3 + 2 = 3\psi\Phi. \tag{17}$$

Form eq. (10) and (14) we know that Φ needs to be as well element of $\mathbb{R}$. This fact is only possible if eq. (16) is limited with

$$\psi > 0. \tag{18}$$

Now eq. (11) and (12) leads to

$$\mathrm{II}_{\mathbf{D}} \leq 0 \tag{19}$$

and with eq. (16), (18) and (19) we can finally predict that the third invariant depends on the second:

$$\left|\mathrm{III}_{\mathbf{D}}\right| \leq \frac{2}{3\sqrt{3}} \left(-\mathrm{II}_{\mathbf{D}}\right)^{\frac{3}{2}}. \tag{20}$$

Fig. 3 shows the possible region of incompressible flow ($\mathrm{I}_{\mathbf{D}} = 0$) in dependence on the second and third invariants. On the edge of the domain, only uniaxial (red) or biaxial (green) elongational flows exist.
Defining the fraction of eq. (20), without the absolute value of the third invariant, leads to

$$\kappa = \frac{\mathrm{III}_{\mathbf{D}}}{\left(-\mathrm{II}_{\mathbf{D}}\right)^{\frac{3}{2}}}. \tag{21}$$

Now the parameter κ is able to describe the elongation fraction of a 3D flow, whereas a 2D flow would generate a zero value for κ. Typical values of basic flow types are listed in Table 2, see Böhme (2000) and Wünsch (2001).

4 Numerical Implementation Techniques

The numerical calculations of the flow of incompressible fluids are based on the equations of continuity and momentum:

$$\nabla \cdot \mathbf{v} = 0, \tag{22}$$

$$\rho \frac{\mathrm{D}\mathbf{v}}{\mathrm{D}t} = -\nabla p + \nabla \cdot \mathbf{T} + \mathbf{f}, \tag{23}$$

where ρ describes the density of the fluid, $\mathrm{D}\mathbf{v}/\mathrm{D}t = \partial\mathbf{v}/\partial t + \nabla \cdot (\mathbf{v} \otimes \mathbf{v})$ is the material time derivative of the Eulerian velocity field $\mathbf{v}$, p denotes the pressure, $\mathbf{f}$ are body forces and $\mathbf{T}$ denotes the total extra stress tensor. In the following, we neglect the body force $\mathbf{f}$ without losing universality.
To include viscoelastic fluid behavior, we first split the extra stress tensor in a Newtonian solvent and a polymer contribution. This is known under the concept of the viscous formulation (VF), see Rajagopalan et al. (1990),

$$\mathbf{T} = \mathbf{T}_\mathrm{s} + \mathbf{T}_\mathrm{p}. \tag{24}$$

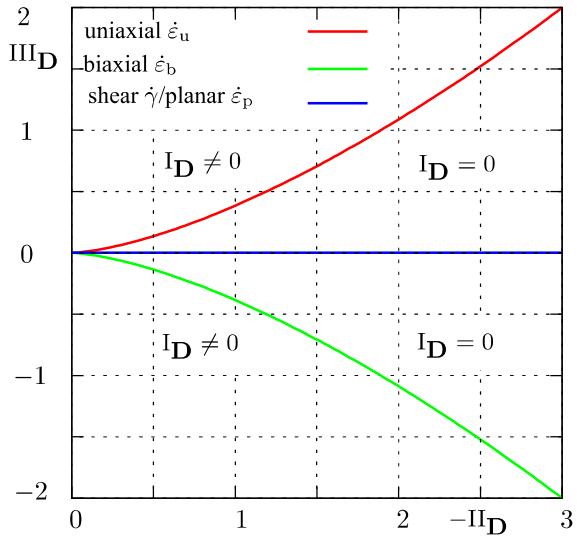

Figure 3: The third invariant of $\mathbf{D}$ as a function of the second invariant of $\mathbf{D}$.

The Newtonian solvent $\mathbf{T}_\mathrm{s}$ is described by a usual linear ansatz with the constant Newtonian viscosity η_s,

$$\mathbf{T}_\mathrm{s} = 2\eta_\mathrm{s}\mathbf{D}. \tag{25}$$

The polymer contribution $\mathbf{T}_\mathrm{p}$ needs a nonlinear relation as shown in eq. (3). With the help of the dimensionalless form of the momentum equation, we are now able to introduce the ratio of Newtonian solvent and polymer contribution

$$\beta = \frac{\eta_\mathrm{s}}{\eta_\mathrm{s} + \eta_\mathrm{p}} \tag{26}$$

to quantify the fraction of viscoelastic stresses. For viscoelastic polymer melts, the parameter β is small. Present works set a value for β that is small enough to describe polymer melts, e. g. $\beta = 1/9$, see Alves et al. (2003); Wünsch (2009).
In order to keep the ellipticity of the equation set (22), (23) and (3) and to guarantee the stability of the numerical simulations using VF methods, β is always greater than zero. The request for numerical stability independent of the parameter β (e. g. for a vanishing β) leads to further developments: the EVSS method (Rajagopalan et al. (1990)) and the Discrete Elastic Viscous Split Stress method (DEVSS), see Guéntte and Fortin (1995). A wide range of modifications of these methods can be found in the literature, see Matallah et al. (1998).
The basic idea of the EVSS method is to further split the polymer contribution in a viscous and an elastic part:

$$\mathbf{T}_\mathrm{p} = \mathbf{T}_\mathrm{v} + \mathbf{T}_\mathrm{e}, \tag{27}$$

where the viscous part of the polymer contribution follows an additional Newtonian ansatz

$$\mathbf{T}_\mathrm{v} = 2\eta_\mathrm{v}\mathbf{D}, \tag{28}$$

with a new viscous viscosity η_v. Including eq. (27) in the generalized Maxwell model eq. (3), with a PTT-L nonlinearity and $\xi = 0$ leads to

$$\mathbf{T}_\mathrm{e} + \lambda\overset{\triangledown}{\mathbf{T}}_\mathrm{e} + \alpha\frac{\lambda}{\eta_\mathrm{p}}\mathrm{tr}\big[\mathbf{T}_\mathrm{e}\big]\mathbf{T}_\mathrm{e} = 2\left(\eta_\mathrm{p} - \eta_\mathrm{v}\right)\mathbf{D} - 2\lambda\eta_\mathrm{v}\overset{\triangledown}{\mathbf{D}} - 2\alpha\frac{\lambda\eta_\mathrm{v}}{\eta_\mathrm{p}}\mathrm{tr}\big[\mathbf{T}_\mathrm{e}\big]\mathbf{D}. \tag{29}$$

On the right side of eq. (29), we now get the upper convected time derivative of the rate of deformation tensor. This leads to a further spatial derivative of the rate of deformation tensor $\mathbf{D}$, viz. second order derivatives of the Euler velocity field. This requires spazial care in numerical calculation methods, as shown in Fortin and Zine (1992). The EVSS method leads to a modified form of the momentum equation

$$\rho\Big(\frac{\mathrm{D}\mathbf{v}}{\mathrm{D}t}\Big) = \nabla p + \left(\eta_\mathrm{s} + \eta_\mathrm{v}\right)\nabla^2\mathbf{v} + \nabla\cdot\mathbf{T}_\mathrm{e}. \tag{30}$$

In order to avoid the problems in calculating the time derivatives of the rate of deformations tensor, Guéntte and Fortin (1995) introduced the rate of deformation tensor $\mathbf{D}$ as an additional unknown. With introducing the elastic part as

$$\mathbf{T}_\mathrm{e} = \mathbf{T}_\mathrm{p} - 2\phi\mathbf{D}, \tag{31}$$

Table 3: Characteristics of the computational meshes used

Mesh	NC	DOF	$\Delta_{\min}$
Mesh A	26000	156000	0.1
Mesh B	104000	624000	0.05
Mesh C	416000	2496000	0.025
Mesh D	310400	1862400	0.0125
Mesh E	986240	5917440	0.00625

we can rewrite (30) to the DEVSS method form of the momentum equation with $\phi = \eta_v$:

$$\rho(\frac{\mathrm{D}\mathbf{v}}{\mathrm{D}t}) = \nabla p + (\eta_s + \eta_v)\nabla^2\mathbf{v} + \nabla \cdot \mathbf{T}_p - \eta_v\nabla^2\mathbf{v}. \tag{32}$$

This null operation enhances the stability in numeric methods noticeably for a wide range of β.

In the following, we use the VF and DEVSS methods implemented to a Finite-Volume simulation code, see Favero (2009a,b); Favero et al. (2009, 2010), which is based on the open source code OpenFOAM, see OpenFOAM (2008). In order to increase the calculation speed, we prefer to use multi-grid methods in case to precondition the matrixes of the linear equation systems. We use the AMG solver, see Jasak et al. (2007). To ensure accuracy, the code and methodology are benchmarked over a wide range of De numbers with the literature Alves et al. (2003); Wünsch (2009); Aboubacar et al. (2002).

5 Benchmark

5.1 Geometry

The contraction problem is often used as a benchmark geometry for non-Newtonian fluids. A viscoelastic fluid passes from one channel or tube into another of smaller dimensions. This entry problem generates complex flow behavior, despite to the simplicity of the geometry: The flow near the wall is dominated by strong shear flow and a uniaxial extension flow is generated along the centreline. Here we have, in a single geometry, two main objects of research in the flow of non-Newtonian fluids.
Because of the different properties of shear and elongation viscosities, the behavior of non-Newtonian fluids is totally different from Newtonian fluids in both regions. In detail, we benchmark our numerical implementation on a two-dimensional 4:1 contraction problem given in Fig. 4. The same conditions for the geometry and viscoelastic models are used in Alves et al. (2003); Wünsch (2009); Aboubacar et al. (2002).

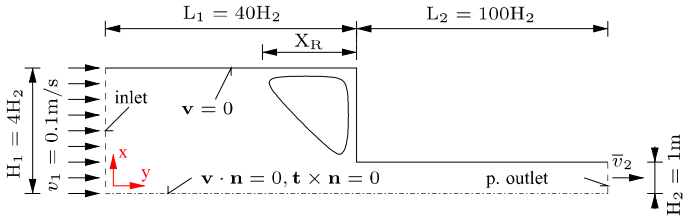

Figure 4: Sketch of the contraction problem.

In order to discretize the calculation domain, we use a structured mesh with different refinements, see Fig. 5.
Table 3 represents the main information of the meshes, where NC is the number of cells, DOF the degree of freedom and the minimum cell spacing is given with $\Delta_{\min} = \Delta\tilde{x} = \Delta\tilde{y}$ where $\tilde{x} = x/H_2$ and $\tilde{y} = y/H_2$.
To describe the character of the flow, we introduce the following dimensionless quantities. The Reynolds number is defined as

$$\mathrm{Re} = \frac{\rho H_2 \overline{v}_2}{\eta} \ll 1, \tag{33}$$

and is held small and constant for all of the simulations in order to ensure creeping flow conditions. As a size for

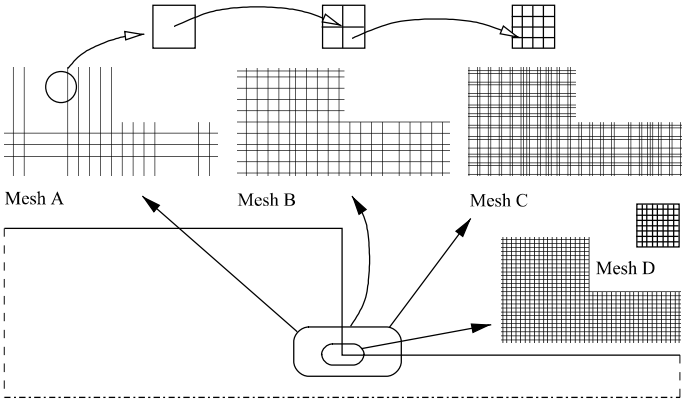

Figure 5: Sketch of the contraction problem and the meshes. Note that each of the refinements of the meshes is four times larger.

the elasticity of a viscoelastic fluid we use the Deborah number

$$\mathrm{De} = \lambda\dot{\gamma} = \lambda\frac{\overline{v}_2}{\mathrm{H}_2}. \tag{34}$$

For the limiting case $\mathrm{De} = 0$, the fluid has Newtonian behavior, elasticity increases as the De number is stepped up. In the following simulations we use the relaxation time λ to set the desired De number.

5.2 Benchmark Results for the Linear and Exponential PTT Fluids

In order to condense the numerical results, first we look at the dimensions of the corner vortex. Fig. 6 show the changes in the size X_R of the vortex defined in Fig. 4. For the PTT-linear model the size increases with increasing De number due to the hardening behavior of the elongational viscosity. At this point, we need to mention that some experimental visualization works show even much higher vortex sizes, see therefore Evans and Walters (1986); Nigen and Walters (2002), and that the linear PTT fluid is not able to supply these Alves et al. (2003). A different behavior is observed when the PTT-exponential model is used. Both the shear and the elongation viscosity decrease at high De numbers and the vortex size decreases to below the Newtonian level following a short rise.
In comparison with the literature Alves et al. (2003), Aboubacar et al. (2002) and Wünsch (2009), the confirmity of the results is shown to be very good. As done in Alves et al. (2003), we average our results over the mesh refinements. Here, only the linear PTT fluid shows big vortex sizes at high De-number. This is, due to the fact that the linear PTT model is sensitive to mesh refinements for higher Deborah numbers.
Fig. 7 shows the development of the vortex size in dependence on minimum cell spacing of the meshes used for our calculations. Fig. 7 shows that only for $\mathrm{De} = 100$ (linear PTT) the result depends on the mesh size distinctly. Note that the meshes used in Alves et al. (2003) have a cell spacing less than $\Delta_{\min} < 0.014$. Furthermore, an excellent agreement is seen in the case of the exponential PTT fluid, see Fig. 7.
Fig. 8 and Fig. 9 show the maximum values of the velocity and stress at the centre line in normalized form:

$$\mathrm{U}_{\max} = \frac{u_{\max}}{\overline{v}_2}, \tag{35}$$

$$\Sigma_{\mathrm{xx}}^{\max} = \frac{\sigma_{\mathrm{xx}}^{\max}\mathrm{H}_2}{3\eta\overline{v}_2}. \tag{36}$$

All models shows similar behavior. For increasing Deborah numbers the values of the extra stress are vanishingly small. The maximum values of the center line velocity show a minimum around a De number of 1. In the case of the linear PTT fluids the refinment of the mesh shows enhancement in the maximum values of the stress and therefore a better agreement with Alves et al. (2003). Finally we can say that the results show good conformity with Alves et al. (2003) and Wünsch (2009).
We also need to mention the well-known singularities at sharp corners as they are evident in the used 4:1 contraction problem in this present work, see Hinch (1993) and Fontelos and Friedman (2000). Through the good stabilization this singularities stays local. In Fiétier and Deville (2002) this problem is solved by rounding the sharp corner. But this includes some changes in the velocity and stress field, see Aboubacar et al. (2002).

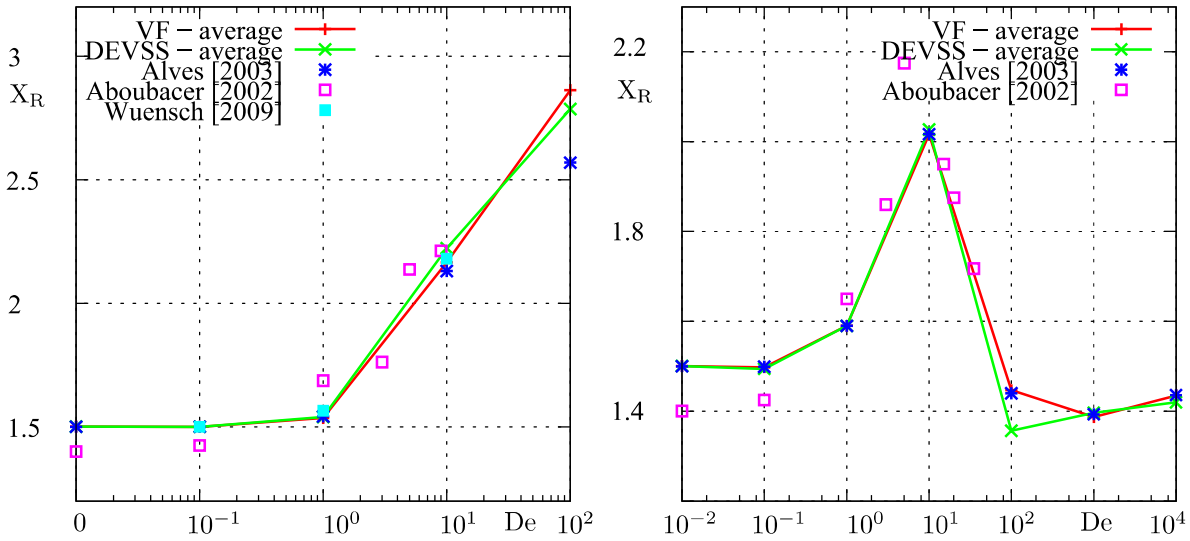

Figure 6: The size of the vortex near the re-entrant corner with the De number (log-scale) for **left:** the linear and **right:** the exponential PTT fluid with $\beta = 1/9$ and $\alpha = 0.25$.

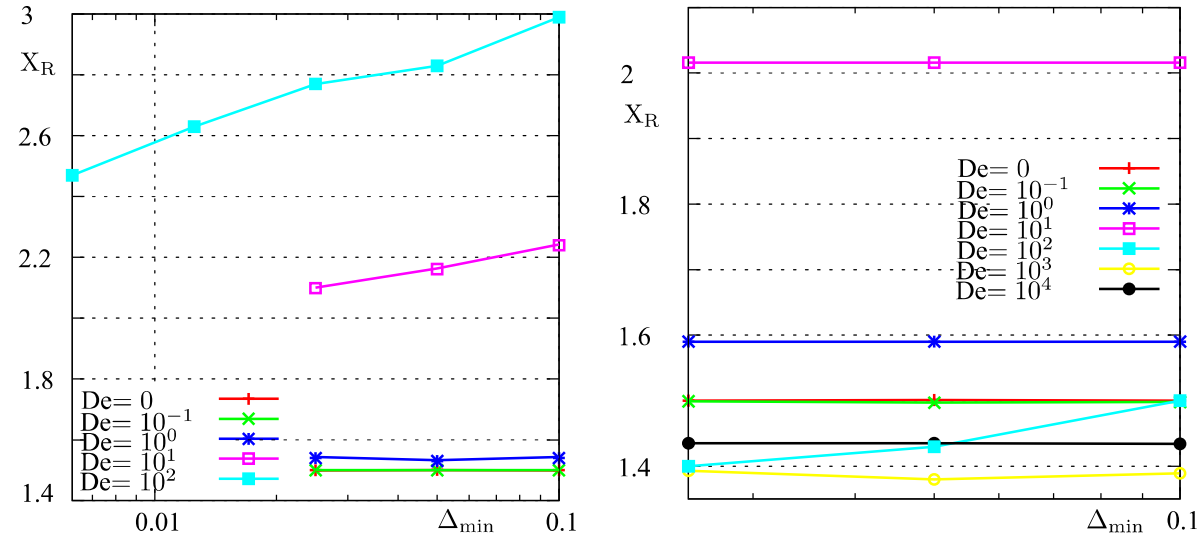

Figure 7: The size of the vortex near the re-entrant corner with the minimum cell spacing (log-scale) for **left:** the linear and **right:** the exponential PTT fluid with $\beta = 1/9$ and $\alpha = 0.25$ and the VF method.

5.3 Further Results for Giesekus Fluids

Fig. 1 have shown that the Giesekus and PTT fluids are similar in the case of basic one-dimensional rheometrical flows. Therefore, the Giesekus model is used for additional calculations in the benchmark geometry. Here, the Giesekus fluid shows an impressive advantage in regard to decribing possible second stress coefficients, see Fig. 2. Furthermore, the accuracy during the numerical calculations over the whole De number, shown in Fig. 10, is not negligible. The similarity to the linear PTT fluids is also demonstrated in Fig. 10 and 6. Fig. 11 show the maximum values at the center line of the velocity and stress. In comparison to the linear PTT fluid we see a good affinity.
The numerical cost related to CPU time is reduced by a factor of 0.4. Furthermore, the stability of the numerical simulations at all Deborah numbers was very high and no additional relaxations where necessary.

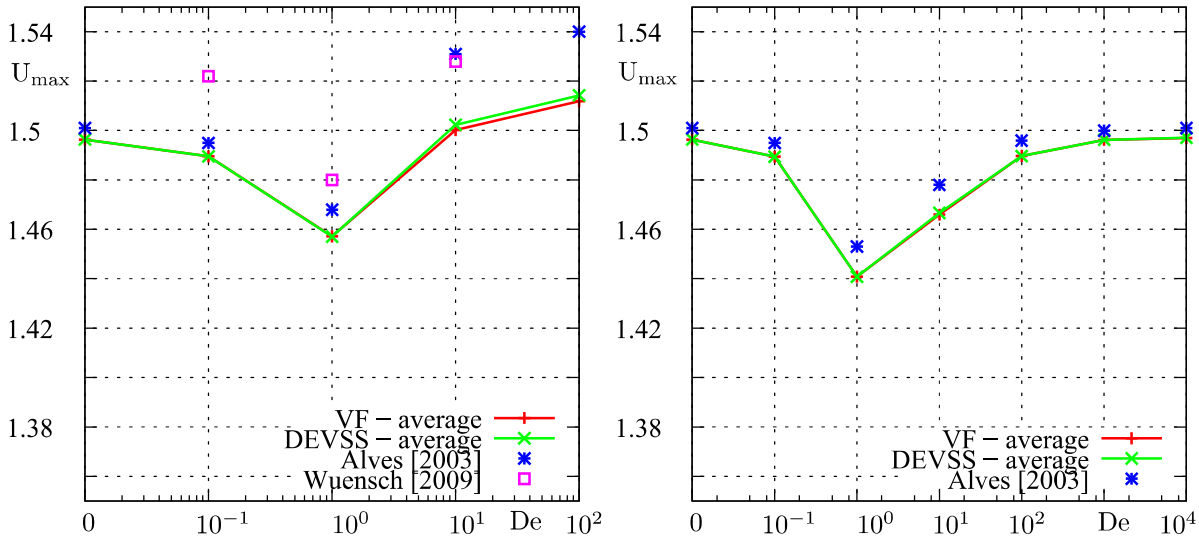

Figure 8: Maximum velocity value along the center line (symmetry axis) with the De number (log-scale) for **left:** the linear and **right:** the exponential PTT fluid with $\beta = 1/9$ and $\alpha = 0.25$.

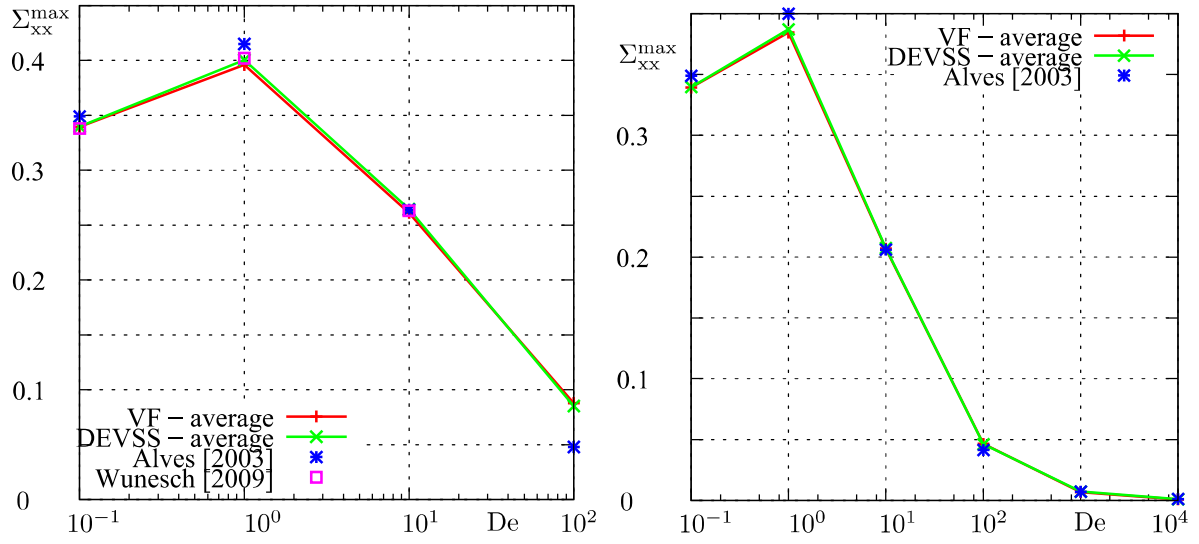

Figure 9: Maximum value of the first extra normal stress along the center line (symmetry axis) with the De number (log-scale) for **left:** the linear and **right:** the exponential PTT fluid with $\beta = 1/9$ and $\alpha = 0.25$.

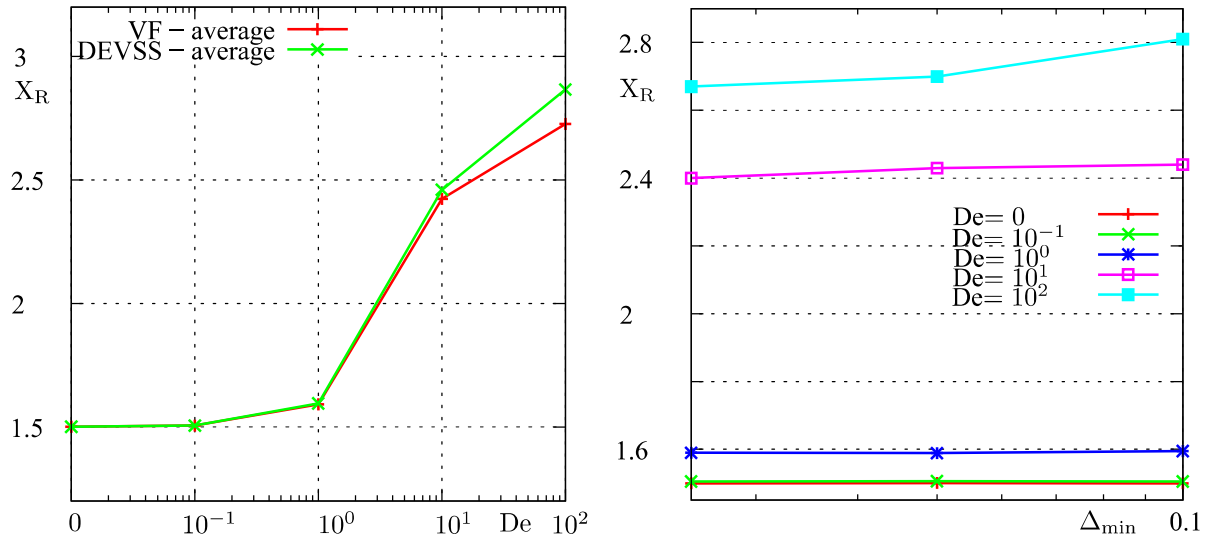

Figure 10: The size of the vortex near the re-entrant corner with the De number (log-scale) and the minimum cell spacing (log-scale) for the Giesekus fluid with $\beta = 1/9$ and $\alpha = 0.25$ and the VF method.

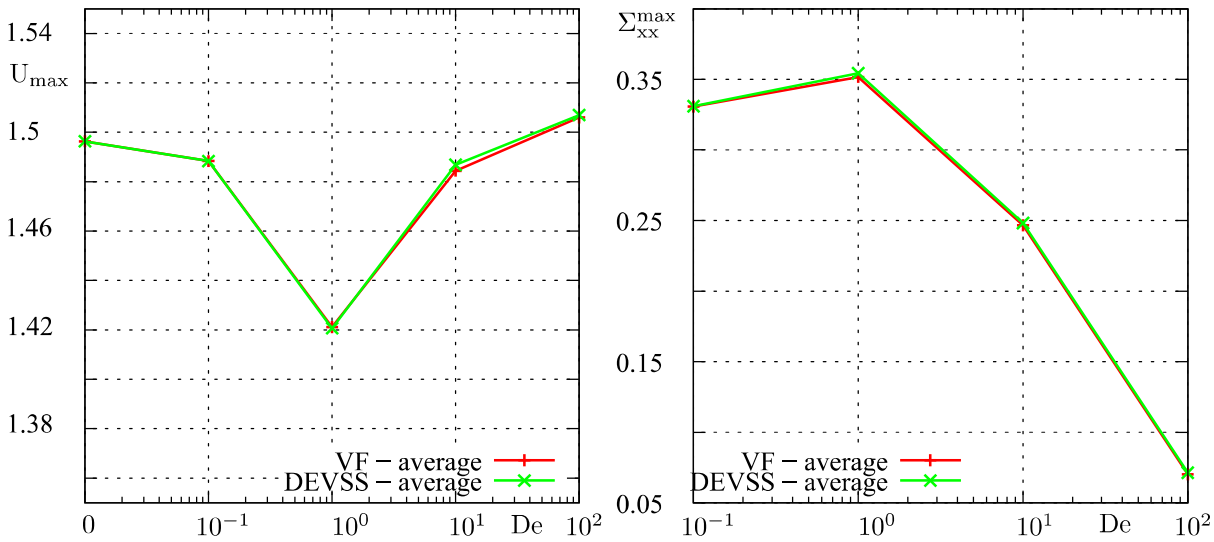

Figure 11: Maximum velocity value and the maximum first extra normal stress value along the center line (symmetry axis) with the De number (log-scale) for the Giesekus fluid with $\beta = 1/9$ and $\alpha = 0.25$.

6 Flow in a Three Dimensional Cross-Slot Geometry

In order to demonstrate the application of the visualization technique explained in chapter 3, we investigate the three dimensional flow in a Cross-Slot geometry. The fluid enters the geometry on two opposite sides and leaves at two outlets in lateral direction. To save memory and computing time, we assume a symmetric fluid flow and use symmetric boundary conditions on different planes. A sketch of the calculation domain is shown in Fig. 12.

The numerical results are visualized on four planes, see Fig. 12. The first visualization plane is the above-mentioned symmetry plane. Behind the symmetry plane we introduce further planes as shown in Fig. 12. All calculations were done at vanishing Re numbers and $\mathrm{De} = 10$.

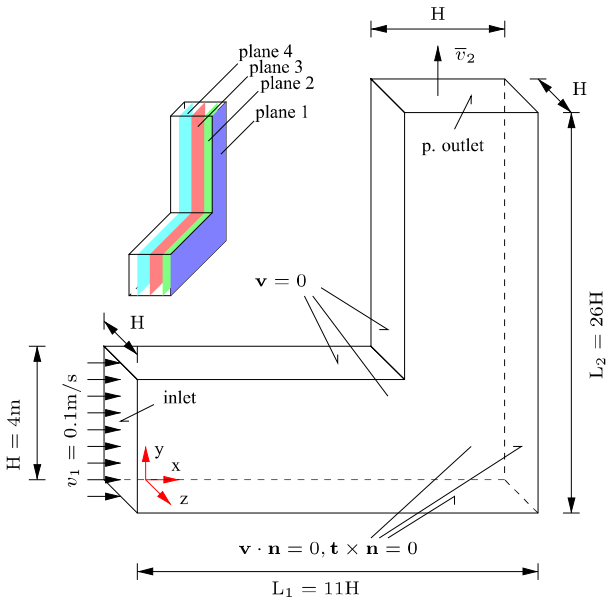

Figure 12: Sketch of the arborization with the boundary conditions used. The mesh is build with 2,304,000 cells.

6.1 Analysis of the Streamlines

First, we investigate the streamlines at the mentioned planes, which are shown in detail near the corner in Fig. 13. In order to demonstrate the influence of the viscoleastic fluid behavior, the Newtonian case is included. All viscoelastic fluids shows similar behavior in the symmetric plane. Minor changes are visible near the change of direction and at the outlet flow. With increasing distance from the symmetric plane, the differences at the corner grows. Here, the influence of the corner becomes more noticeable, as showon also in Fig. 14 and Fig. 15. Furthermore, the streamlines of the exponential form of the PTT fluids are much closer to the Newtonian case. Here, the increase in differences in three dimensions are due to the fact that different types of models have different nonlinearity tensorial functions.

6.2 Visualization of the Flow Type

In order to discuss the flow type, we visualize the flow type parameter defined in eq. (21) at plane 2-4, see Fig. 12. In Fig. 14, plane 3 is shown and the values of the flow type are listed in Table 2. In a Newtonian fluid, the fluid type parameter shows an antisymmetric behavior. Coming from the left, the fluid is only sheared (green, $\kappa = 0$) until the arborization begins. Here a biaxial elongation flow (blue) develops near the center line and a small domain with uniaxial elongation flow (red) appears near the wall. Then the flow merges to a planar elongation type (green) near the crosspoints of the center lines. After crossing the antisymmetric line the flow type changes accordingly. Viscoelastic fluids break the antisymmetry. Looking at the biaxial regions, the small region near the wall grows in comparison to the Newtonian fluid and the lower region near the center line is more thronged to the left. The uniaxial regions are swayed in the same way. First, the big region is moved to the right side and is warped to the

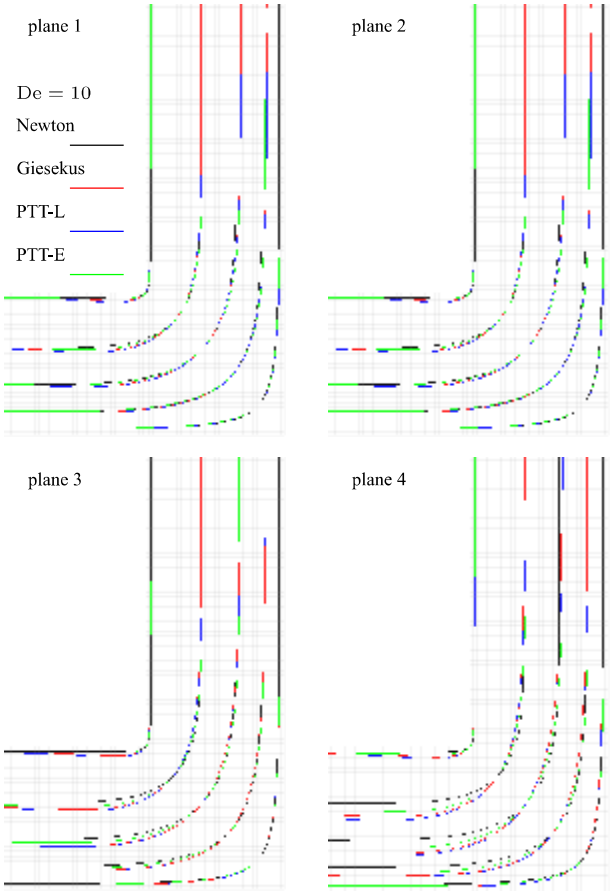

Figure 13: Streamlines of the 3D Cross-Slot geometry at the planes 1-4 (Fig. 12).

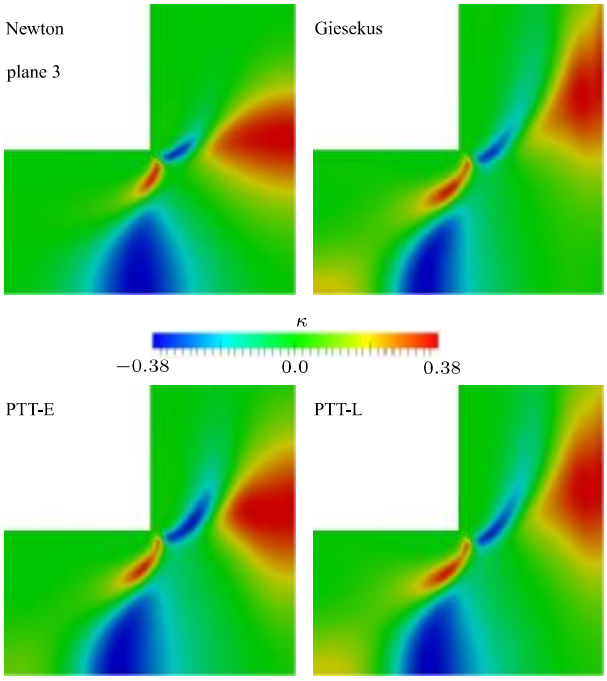

Figure 14: Flow type parameter κ, at $\mathrm{De} = 10$ using the VF method in plane 3.

downstream region. The small upper uniaxial region increases and now a big region appears on the left side even before the big biaxial region.
Only minor differences in the flow type are visible between the linear PTT and Giesekus fluids. The flow type of

the exponential form of the PTT fluids looks similar to the Newtonian case. This can be explained by the different viscosity behavior for shear and elongation flow. All viscoelastic models shows shear-thinning behavior for the shear viscosity; in the case of elongation viscosity, the linear PTT and Giesekus fluids are of hardening nature, see Fig. 1.
In contrast, the elongation viscosity of the exponential PTT fluid decreases for higher elongation rates. Obviously, the different elongation viscosity behavior of the models at higher elongation rates is responsible for the break of the antisymmetry. This is confirmed in Fig. 15, where the flow type parameter is shown for Newtonian and Giesekus fluid in planes $2-4$.
The use of different material models have not only an influence to the flow pattern, but also the pressure difference

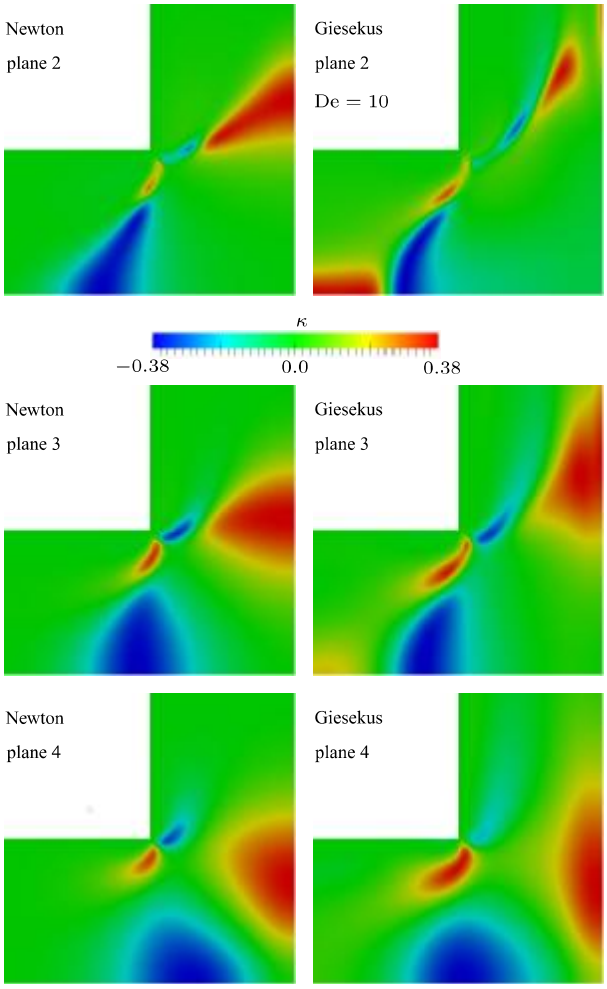

Figure 15: Using κ to show the unsymmetric behavior of the uniaxial and biaxial regions of a Giesekus fluid. Note, that the small uniaxial elongation flow region of the Giesekus Fluid (at the upper right corner in plane 2) gets bigger and merges, see plane 3.

$$\Delta\tilde{p} = \frac{p\mathrm{H}}{\eta v_1} \tag{37}$$

between the in- and outlet of the geometry is different, see Table 4. Due to the shear thinning behavior of the shear viscosity of all the viscoelastic models, the pressure difference is reduced in comparison with the Newtonian fluid.

7 Conclusions

The main idea of the work is to understand the influence of elasticity of viscoelastic fluids on the flow pattern in technical apparatus. The flow types of Newtonian and highly viscoelastic fluids can be visualized in numerical works with the help of the invariants of the rate of deformation tensor. The use of invarinats is attractive and helpful because they are independent of any changes in the coordinate system. This method only requires knowledge of

Table 4: Normalized pressure difference, see eq. (37)

Model	$\Delta\tilde{p}$
Newton	4.29
Giesekus	0.65
PTT-L	0.71
PTT-E	0.84

the velocity field. It is universally deployable, because it is independent of the extra stress tensor or the model used. With the help of the flow type parameter it is possible to show how the elasticity of a fluid changes the flow type regions in comparison with the Newtonian case.
Knowing the real material behavior of viscoelastic fluids in shear flows and uniaxial and biaxial elongations is important for choosing the right model to describe the viscoelastic properties of the fluid. In McLeish and Larson (1998) and Isaki et al. (1991) it has been shown that the biaxial elongation viscosity is similar to the uniaxial elongation viscosity. Hence, the material model can be chosen to describe one of these viscosities and the other is done without more effort.
The flow type parameter can be applied effected in two steps. First, a simulation of the flow is made with a Newtonian fluid. This is normally done without a lot of numerical efforts. By visualizing κ we are able to predict the regions of interest in a viscoelastic simulation.
This Newtonian simulation helps to provide assurance about the regions and the domination of elongation and or shear flow type. With this knowledge, the right choice of the material model should be safer to make. For the numerical calculation done in this work we conserve the ellipticity of the governing equations using VF and DEVSS methods. The codes used have good conformity with the benchmark tests in literature over a wide range of Deborah numbers.

Acknowledgements The authors wish to thank J. Favero, Federal University of Rio de Janeiro, for the helpful discussions. The project is financially supported by the German Research Funding Organistaion (DFG).

References

Aboubacar, M.; Matallah, H.; Webster, M.: Highly elastic solutions for Oldroyd-B and Phan-Thien/Tanner fluids with a finite volume/element method: planar contraction flows. *Journal of Non-Newtoninan Fluid Mechanics*, 103, (2002), 65–103.

Alves, M.; Oliveira, P.; Pinho, F.: Benchmark solutions for the flow of Oldroyd-B and PTT fluids in planar contractions. *Journal of Non-Newtoninan Fluid Mechanics*, 110, (2003), 45–75.

Bird, B.; Armstrong, R.; Hassager, O.: *Dynamics of Polymeric Liquids*. John Wiley, New York (1987).

Böhme, G.: *Strömungsmechanik nichtnewtonscher Fluide*. Teubner, Leipzig (2000).

Dhanasekharan, M.; Haung, H.; Kokini, J.: Comparison of Observed Rheological Properties of Hard Wheat Flour Dough With Predictions of the Giesekus-Leonov, White-Metzner and Phan-Thien Tanner Models. *Journal of Texture Studies*, 30, (1999), 603–623.

Evans, R.; Walters, K.: Flow characteristics associated with abrupt changes in geometry in the case of highly elastic liquids. *Journal of Non-Newtonian Fluid Mechanics*, 20, (1986), 11–29.

Favero, J.: Simlaçã de Escoamentos Viscoelásticos Desenvolvmento de uma Metodologia de Anaálise utilizando o Software OpenFOAM e Equações Constitutivas Diferenciais (2009a), Master Theses, Universidade Federal do Rio Grande do Sul.

Favero, J.: Viscoelastic Flow Simulation in OpenFOAM, Presentation (2009b), Universidade Federal do Rio Grande do Sul.

Favero, J.; Secchi, A.; Cardozo, N.; Jasak, H.: Viscoelastic flow simulation: development of a methodology of analysis using the software OpenFOAM and differential constitutive equations. *10th International Symposium on Process Engineering-PSE2009*, pages 915–920.

Favero, J.; Secchi, A.; Cardozo, N.; Jasak, H.: Simulation of Free Surface Viscoelastic Fluid Flow Using the viscoelasticInterFoam solver. *20th European Symposium on Computer Aided Process Engineering-ESCAP20*.

Fiétier, N.; Deville, M.: Simulations of Time-Dependent Flows of Viscoelastic Fluids with Spectral Element Methods. *Journal of Scientific Computing*, 30-1-4, (2002), 649–657.

Fontelos, M.; Friedman, A.: The Flow of a class of Oldroyd Fluids around a re-entrant corner (2000), Institute for Mathematics and its Applications, University of Minnesota–IMA Preprint Series-1684.

Fortin, A.; Zine, A.: An Improved GMRES Method for Solving Viscoelastic Fluid Flow Problems. *Journal of Non-Newtonian Fluid Mechanics*, 42, (1992), 1–18.

Giesekus, H.: A Simple Constitutive Equation For Polymer Fluids Based on The Concept of Deformation-Dependent Tensorial Mobility. *J. of Non-Newt. Fluid Mechanics*, 11, (1982), 69–109.

Giesekus, H.: *Phänomenologische Rheologie*. Springer, Berlin (1994).

Guéntte, R.; Fortin, M.: A new mixed finite element method for computing viscoelastic flows. *Journal of Non-Newtoninan Fluid Mechanics*, 60, (1995), 27–52.

Hasseger, O.; McKinley, G.; Nielsen, J.; Rasmussen, H.: Elongational viscosity of monodisperse and bidisperse polystyrene melts. *Hatsopouls Microfluids Laboratory*, HML Report 06-P-06.

Hinch, E.: The flow of an Oldroyd fluid around a sharp corner. *Journal of Non-Newtoninan Fluid Mechanics*, 50, (1993), 161–171.

Isaki, T.; Takahashi, M.; Takigawa, T.; Masuda, T.: Comparison between uniaxial and biaxial elongational flow behavior of viscoelastic fluids as predicted by differential constitutive equations. *Rheologica Acta*, 30, (1991), 530–539.

Jasak, H.; Jemcov, A.; Maruszewski, J. P.: Preconditioned Linear Solvers for Large Eddy Simulation, CFD 2007 Conference, CFD Society of Canada (2007).

Jin, H.; Thien, N.; Tanner, R.: A finite element analysis of the flow past a sphere in a cylindrical tube: PTT fluid model. *Computational Mechanics*, 8, (1991), 409–422.

Joseph, D.; Renardy, M.; Saut, J.: Hyperbolicity and Change of Type in the Flow of Viscoelastic Fluids. *Archive for Rational Mechanics and Analysis*, 87, (1985), 213–251.

Joseph, D.; Yoo, J.: Hyperbolicity and Change of Type in The Flow of Viscoelastic Fluids Through Channels. *Journal of Non-Newtonian Fluid Mechanics*, 19, (1985), 15–41.

Keyfitz, B.; Shearer, M.: *Nonlinear Evolution Equations That Change Type*. Springer, Berlin (1990).

Matallah, H.; Townsend, P.; Webster, M.: Recovery and stress-splitting schemes for viscoelastic flows. *Journal of Non-Newtoninan Fluid Mechanics*, 75, (1998), 139–166.

McLeish, T.; Larson, R.: Molecular constitutive equations for a class of branched polymers: The pom-pom polymer. *Journal of Rheology*, 42-1, (1998), 81–110.

Muniz, A.; Sechi, A.; Cardozo, N.: High-Order Finite Volume Method for Solving Viscoelastic Fluid Flows. *Brazilian Journal of Chemical Engineering*, 25-1, (2008), 153–166.

Nigen, S.; Walters, K.: Viscoelastic contraction flows: comparison of axisymmetric and planar configurations. *Journal of Non-Newtonian Fluid Mechanics*, 102, (2002), 343–359.

Oldroyd, J.: On the Formulation of Rheological Equations of State. *Proceedings of the Royal Society*, 200, (1950), 523–541.

OpenFOAM: The Open Source CFD Toolbox (2008), User Guide 1.5.

Rajagopalan, D.; Armstrong, R.; Brown, R.: Finite Element Methods for Calculation of Steady, viscoelastic Flow using a constitutiv Equations with a Newtonian Viscosity. *Journal of Non-Newtonian Fluid Mechanics*, 36, (1990), 159–192.

Renardy, M.: Existence of Slow Steady Flows of Viscoelastic Fluids with Differential Constitutive Equations. *ZAMM*, 65-9, (1985), 449–451.

Thien, N.: A nonlinear network viscoelastic model. *J. Rheo.*, 22(3), (1978), 259–283.

Thien, N.; Tanner, R.: A new constitutive equation derived from network theory. *J. of Non-Newt. Fluid Mechanics*, 2, (1977), 353–365.

Wünsch, O.: *Strömungsmechanik des laminaren Mischens*. Springer, Berlin (2001).

Wünsch, O.: Laminar Fluid Flow with Complex Material Behavior in Devices of Mechanical Engineering. *International Journal of Emerging Multidisciplinary Fluid Sciences*, 1-4, (2009), 255–267.

Xue, S.; Thien, N.; Tanner, R.: Three diemensional numerical simulation of viscoelastic flows through planar contractions. *Journal of Non-Newtoninan Fluid Mechanics*, 74, (1998), 195–245.

Address: Dipl.-Ing. A. Abid (Al-Baldawi), Institute of Mechanics, University of Kassel, D-34125 Kassel.
email: ammar@uni-kassel.de